Journal of Nanoparticle Research (2006) 8:995–1002
DOI 10.1007/s11051-006-9111-8

Nanoparticle-coated silicon nanowires

J. Hafiz*, R. Mukherjee, X. Wang, M. Cullinan, J.V.R. Heberlein, P.H. McMurry and S.L. Girshick
*Department of Mechanical Engineering, University of Minnesota, 111 Church St. SE, Minneapolis, 55455, Minnesota, USA; *Author for correspondence (E-mail: jhafiz@me.umn.edu)*

Received 19 October 2005; accepted in revised form 4 April 2006

Key words: silicon nanowire, particle impaction, faceted catalyst, thermal plasma, hybrid nanostructure, coating, aerosols

Abstract

The synthesis of silicon nanowires that are densely coated with silicon nanoparticles is reported. These structures were produced in a two-step process, using a method known as hypersonic plasma particle deposition. In the first step, a Ti–Si nanoparticle film was deposited. In the second step the Ti-source was switched off, and nanoparticle-coated nanowires grew under the simultaneous action of Si vapor deposition and bombardment by Si nanoparticles. Total process time, including both steps, equaled 5 min, and resulted in formation of a dense network of randomly oriented nanowires covering $\sim$1.5 cm^2 of substrate area. The nanowires are composed of single-crystal Si. The diameters of the nanowires vary over the range $\sim$100–800 nm. Each nanowire has a crystalline $TiSi_2$ catalyst particle, believed to have been solid during nanowire growth, at its tip.

Introduction

Hybrid nanostructures consisting of nanotubes or nanowires that are decorated or completely coated with nanoparticles are of interest for a variety of potential applications, including catalysis, sensors, electronic devices, magnetics, optics and others. A number of investigators have reported decorating carbon nanotubes with metal nanoparticles (Planeix et al., 1994; Zhang et al., 2000a, 2000b; Kong et al., 2001; Choi et al., 2002; Jiang et al., 2003; Ye et al., 2003; Ye et al., 2004). Several different methods were used to achieve the nanoparticle decoration, including liquid solution methods (Planeix et al., 1994; Choi et al., 2002; Jiang et al., 2003), electron beam evaporation (Zhang et al., 2000a; Kong et al., 2001), physical vapor deposition (Zhang et al., 2000b) and supercritical carbon dioxide (Ye et al., 2003, 2004). More recently the coating of various types of nanowires with nanoparticles has been reported. Dense coatings of nickel and platinum nanoparticles were deposited onto silicon carbide nanowires by plasma-enhanced chemical vapor deposition (LaLonde et al., 2005). Physical vapor deposition was used to grow platinum nanoparticles on SnO_2 nanowires and nanobelts (Kolmakov et al., 2005). Polyaniline nanofibers were decorated with gold nanoparticles using a redox reaction with chloroauric acid (Tseng et al., 2005). Epitaxial germanium islands were grown on silicon nanowires using chemical vapor deposition (Pan et al., 2005). In all of the work cited above, both for nanotubes and for nanowires, the nanoparticle coating was achieved by a heterogeneous gas/solid or liquid/solid reaction at the nanotube or nanowire surface, in which the nanoparticles nucleated and grew as discrete islands on the surface.

In another approach, ZnO nanoparticles were externally injected into a network of ZnO

nanowires using liquid solutions of the nanoparticles (Baxter & Aydil, 2006). The goal was to develop hybrid morphologies that would exploit both the high surface area of nanoparticles and electron transport along a nanowire network, in the context of dye-sensitized solar cells. Depending on properties of the solution, the authors obtained either a sparse coverage of nanoparticles attached to the nanowires, a dense coating of nanoparticles, only some of which were attached to the nanowires while others filled the void spaces between nanowires, or nanoparticles sitting on top of the nanowire network.

In this paper we report the synthesis of Si nanowires that are densely coated with Si nanoparticles. During growth the nanowires are exposed to bombardment by nanoparticles from the gas phase, and we believe that this is the primary source of the nanoparticle coating. To our knowledge coating of nanowires with nanoparticles that bombard the nanowires from the gas phase has not previously been reported.

These structures were deposited using a process known as hypersonic plasma particle deposition (HPPD). Initially the nanoparticle-coated nanowires were produced by serendipity, in an experiment designed to produce a graded-composition nanoparticle film not nanowires. Thereafter the same experimental conditions were run several times, and the results were found to be reproducible.

Experimental

In HPPD nanoparticles are synthesized by gas-phase nucleation in the rapid nozzle expansion of a thermal plasma with injected chemical reactants. The particles are accelerated in the hypersonic expansion, and impact the substrate to be coated at velocities up to $\sim$2 km/s, creating a dense nanoparticle film. The HPPD apparatus is described in detail elsewhere (Rao et al., 1998; Blum et al., 1999; Girshick et al., 2002).

In these experiments the plasma was generated by a direct-current arc operating at 200–275 A current and $\sim$8 kW power input. The main plasma gases were argon, at a flow rate of 30 slm, and hydrogen, at 2–3 slm. A two-step process was used. In the first step, which lasted for 2 min, vapors of $SiCl_4$ and $TiCl_4$ were co-injected into the plasma at flow rates of 20 and 40 sccm, respectively. In the second step, which lasted for 3 min, the $TiCl_4$ flow was switched off, and the $SiCl_4$ flow rate was increased to 40 sccm. These gases were injected at the upstream end of the expansion nozzle, at a location where the plasma temperature is $\sim$4000 K, high enough to completely dissociate the reactants. The pressure at the location of reactant injection equaled $\sim$60 kPa, dropping to 267 Pa in the expansion chamber. A molybdenum substrate was positioned in the expansion chamber 20 mm downstream of the nozzle exit. The substrate temperature was maintained at 1230 K (film deposition surface) using a previously described temperature-control system (Bieberich & Girshick, 1996).

Deposits were examined *ex-situ* by scanning electron microscopy (SEM) using a JEOL 6500 field emission microscope equipped with an energy dispersive spectrometer (EDS). For transmission electron microscopy we used a dedicated analytical microscope, VG HB501 STEM (Scanning Transmission Electron Microscope). A FEI Tecnai G2 F30 microscope was used for high-resolution transmission electron microscopy (HRTEM). Samples for TEM were prepared by scraping the material from the substrate into acetone and then depositing a few drops onto carbon grids for imaging.

Results and discussion

Figure 1a shows an SEM image of a film for which only the first step of the process was conducted, co-injection of $SiCl_4$ and $TiCl_4$ for a period of 2 min, resulting in a film of nanoparticles. As can be seen the particles are rather monodisperse, with most particles having a diameter in the range 30–40 nm. An X-ray diffraction spectrum of this film (Figure 1b), indicates peaks associated with crystalline Si, $TiSi_2$ and Ti_5Si_3. We believe that the Si peak is attributable to the presence of silicon nanoparticles in the film.

In the second step of the process, with the $TiCl_4$ flow switched off and the $SiCl_4$ flow rate doubled, a dense array of randomly oriented nanowires grew on top of the Ti–Si nanoparticle film, as seen in Figure 2. The nanowire deposit covered $\sim$1.5 cm^2 of the substrate. Calculated mass deposition rates of the nanowires equal approximately

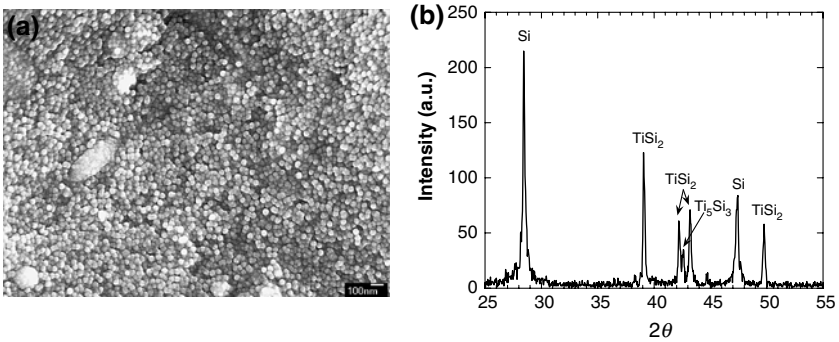

Figure 1. (a) SEM image of Ti–Si nanoparticle film produced in Step 1 before nanowire growth (b) X-ray diffraction spectrum of the same film.

1 mg/h. Previous publications on high-yield synthesis of Si nanowires have reported deposition rates of 0.1–1 mg/h (Wang et al., 1998; Zhang et al., 1998; Rao et al., 2003), although it should be noted that the nanowires reported here are thicker than in those studies.

Figure 3 shows SEM images of the same deposit at higher resolutions. The diameters of the nanowires vary over the range ~100–800 nm. In Figure 3(a) it is seen that the majority of the nanowires contain bends, suggesting that they are not defect-free. In this figure, and especially in Figure 3(b), it can be seen that each nanowire has a faceted catalyst particle at its tip. Figure 4 shows high-resolution SEM images, at two different magnifications, of a single nanowire, which is seen to be densely coated with nanoparticles whose diameters appear to lie in the range ~5–25 nm.

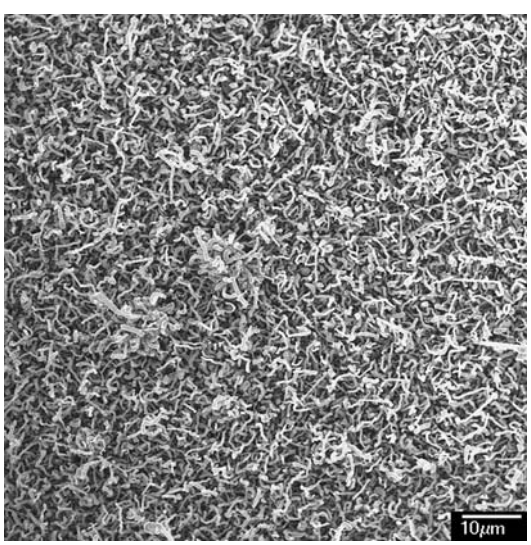

Figure 2. Low-resolution SEM image of nanowire array.

An EDS linescan was obtained using the STEM analytical microscope on a single nanowire with an intact catalyst tip. The result, shown in Figure 5, indicates that the particle at the tip consists of $TiSi_2$, while the body consists only of Si. It is known that $TiSi_2$ catalyzes the growth of silicon nanowires (Kamins et al., 2000).

The fact that the catalyst particles are faceted crystallites not spheres suggests that nanowire growth occurred by diffusion of Si vapor through solid catalyst particles, rather than following the more common vapor–liquid–solid (VLS) mechanism (Wagner & Ellis, 1964). Previous studies have demonstrated that Si nanowire growth can be catalyzed by solid $TiSi_2$ particles (Kamins et al., 2000, 2001), and this hypothesis is supported by the fact that the deposition temperature, 1230 K, was significantly below the lowest liquid eutectic temperature in the Ti–Si system, 1605 K (Massalski et al., 1986).

To characterize the underlying nanowire structure we followed two approaches. The first was to examine the large-scale structure of individual nanowires by means of dark-field TEM images. Figure 6 shows both a bright-field image and a dark-field image of rod-like nanowires that were scraped onto TEM grids. The large nanorod "lights up" in the dark-field image along its entire length, indicating that it contains a single-crystal core with a common orientation with respect to the electron beam.

A second approach that proved fruitful was to locate a region of a nanowire that did not contain

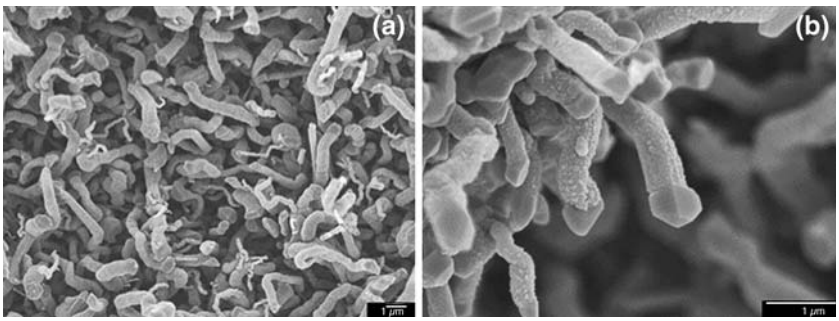

Figure 3. (a) Nanowires contain kinks and bends. (b) Each nanowire contains a faceted catalyst particle at its tip.

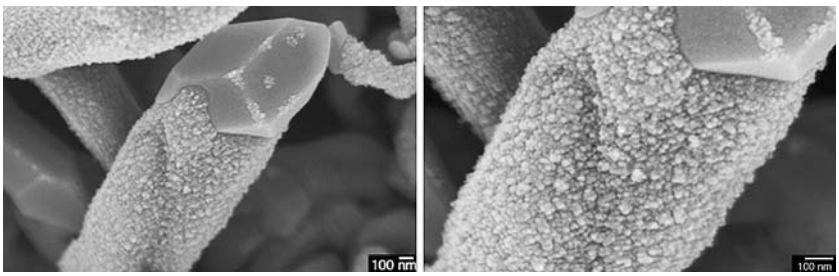

Figure 4. High-resolution SEM images of a nanoparticle-coated nanowire (20 kV electron beam energy).

the nanoparticle coating. Figure 7(a) shows a nanowire with a bare area without the nanoparticle coating, while Figure 7(b) shows a high-resolution TEM image of that area. The lattice parameter of the crystal was determined by analyzing the lattice plane spacing from the HRTEM image. The calculated lattice spacing equals 0.315 nm, closely corresponding to the theoretical value of 0.314 nm of (111)-Si. However, the nanowires are not defect-free, as can be observed in Figure 7(c), which shows the presence of multiple stacking faults in a different region of the bare spot.

While the detailed mechanism for formation of the nanoparticle-coated nanowires reported here is not known, it is reasonable to hypothesize that the growth mechanism is related to the unusual nature of the HPPD growth environment, which, depending on conditions, can involve simultaneous nanoparticle impact and chemical vapor deposition. In HPPD, nanoparticles nucleate in the nozzle expansion and bombard the substrate by hypersonic impaction, producing nanoparticle films such as the underlying Ti–Si film, shown in Figure 1a, that is produced in the first step of the nanowire growth process. At the same time, the gas phase environment adjacent to the substrate may be conducive to chemical vapor deposition. For the operating conditions of these experiments a stationary bow shock lies ~2 mm above the substrate, where the hypersonic free jet has expanded to approximately Mach 8. Numerical modeling (Gidwani, 2003) predicts that the gas is cold in the hypersonic flow just upstream of the shock, but past the shock the temperature rapidly recovers almost to its stagnation value, i.e. to the ~4000 K value at the inlet of the expansion nozzle, before dropping to the substrate temperature, in these experiments ~1230 K (during deposition the distance from the nozzle to the substrate is 20 mm). Thus the temperature at the edge of the fluid boundary layer above the substrate is quite high, and the temperature gradient is extremely steep. If, for example, Si-containing species are not completely consumed by gas-to-particle conversion upstream of the shock, then under these conditions one would expect the substrate to be exposed to high fluxes of monatomic Si vapor, which would be expected to be an active growth species for nanowire growth if suitable catalyst particles are present.

To verify that nanoparticles do indeed bombard the substrate under conditions of the second step

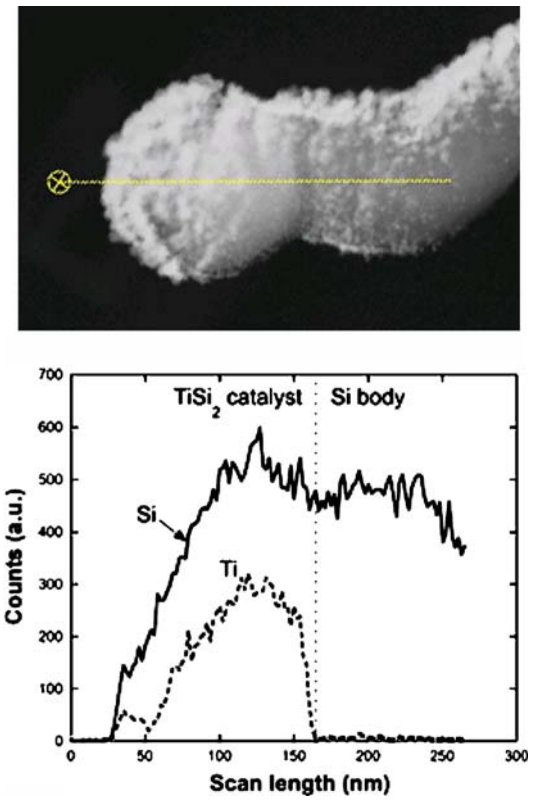

Figure 5. STEM image of a nanowire with EDS linescan to determine the elemental composition of the catalyst particle and the nanowire body. The scan was taken along the line shown on the STEM image.

of the nanowire growth process, and to characterize their size distribution, separate experiments were conducted. With all conditions the same as in the second step of the process, the substrate was removed, and a capillary sampling probe was placed at the same location as that of the substrate during the nanowire growth experiments. The sampled aerosol was rapidly diluted and then delivered to a scanning mobility particle sizer (SMPS), which provided measurements of concentrations and size distributions of the sampled nanoparticles. A detailed description of this system is presented elsewhere (Wang et al., 2005).

Figure 8 shows the particle size distribution measured by the SMPS system. These measurements indicate that the total particle concentration at the sampling location equaled 2.8×10^8 cm^{-3}, the number-mean particle diameter equaled 6.6 nm, and the volume-mean particle diameter equaled 13.0 nm. As the only reactant here was $SiCl_4$, these particles are expected to be Si, perhaps with some level of hydrogenation. (Cl is removed by hydrogen in the flow as gaseous HCl.) For conditions of our experiments, numerical simulations (Gidwani, 2003) indicate that the cut size for inertial impaction of Si particles at the location of the substrate equals $\sim$4 nm, roughly corresponding to the lower detection limit of the SMPS system. Thus virtually all of the particles shown in the size distribution in Figure 8 can be expected to impact the growing nanowire network, with high efficiency. While it is difficult to relate the measured size distribution directly with the SEM images in Figure 4, it seems plausible that the nanoparticle coating on the nanowires results directly from this nanoparticle bombardment. While the particles seen in the SEM images seem

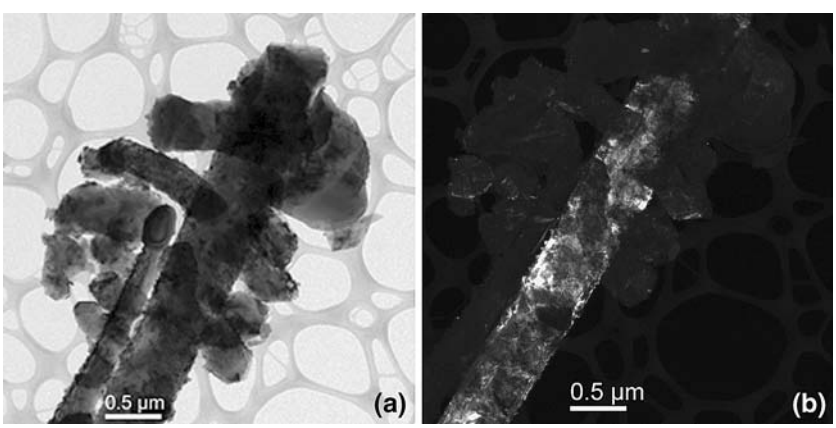

Figure 6. (a) Bright-field TEM image shows several nanowires scraped onto TEM grid. (b) Dark-field image of same area. The large nanorod lights up along its entire length, indicating that it is a single crystal.

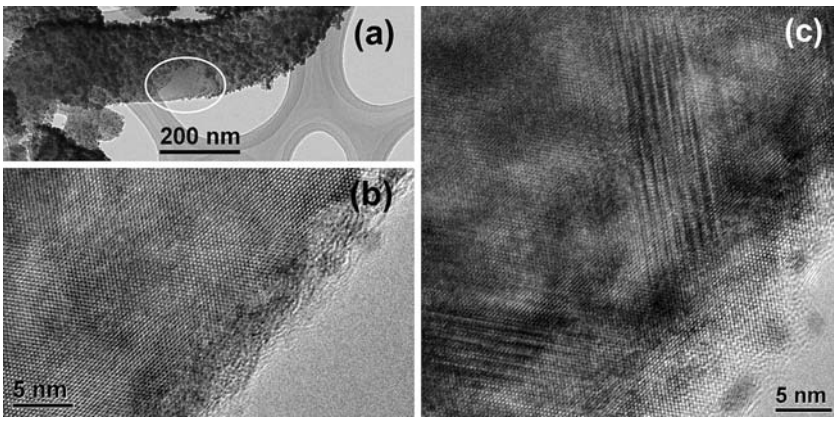

Figure 7. (a) Oval on TEM image highlights bare area of nanowire, without nanoparticle coating. (b) HRTEM image of the bare area reveals the crystalline structure. (c) In a different region of the bare area stacking faults are evident. The TEM electron beam energy was 300 kV.

somewhat larger than those represented by the size distribution measured by SMPS, it should be noted that some of the grains seen in Figure 4 may themselves be agglomerates of smaller particles. Furthermore, once nanoparticles stick to the nanowires it is possible that they continue to grow by vapor deposition.

Our proposed growth mechanism is illustrated in Figure 9. In the first step in the deposition process, a mixed-composition Ti–Si nanoparticle film is deposited. Many of these particles are composed of stoichiometric $TiSi_2$, while others may be sub-stoichiometric on impact but then convert to $TiSi_2$ under exposure to a flux of Si vapor. These $TiSi_2$ particles then grow larger by high-temperature sintering. To our knowledge sintering of nanoscale $TiSi_2$ has not previously been studied. However, this seems the most likely mechanism to explain the growth of the $TiSi_2$ particles from the 30–40-nm size seen in Figure 1a to the hundreds-of-nm sizes seen in Figures 3 and 4. The temperature of the substrate during film growth, 1230 K, is plausibly high enough to accomplish this, while the 2-min duration of the first step may be too brief for such substantial grain growth to have occurred.

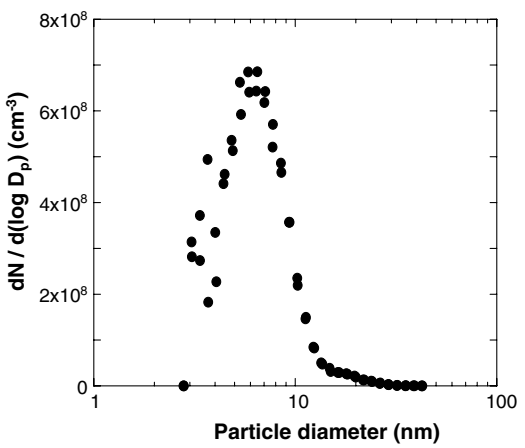

Figure 8. Measured size distribution of particles sampled from the flow at the same location as the substrate for nanowire growth, and for the same conditions as step 2 of the nanowire deposition process.

Nanowires grow by exposure of the $TiSi_2$ catalyst particles to Si vapor in the second step of the process. At the same time, Si nanoparticles that bombard the substrate preferentially stick to the nanowire surfaces. As this bombardment is unidirectional, oriented normal to the substrate, it is perhaps surprising that the nanowires appear to be completely coated with nanoparticles, i.e. one does not observe any shadowing effect. We suggest that the impacting nanoparticles, arriving at velocities around 2 km/s, bounce off the underlying nanoparticle film, and that they are more likely to stick to the nanowires than to either the underlying film or the $TiSi_2$ catalyst particles. This, together with the high density of nanowire coverage, could explain the fact that the nanowires are densely coated with nanoparticles, whereas the spaces between the nanowires are not filled with nanoparticles, and the surfaces of the $TiSi_2$ catalyst

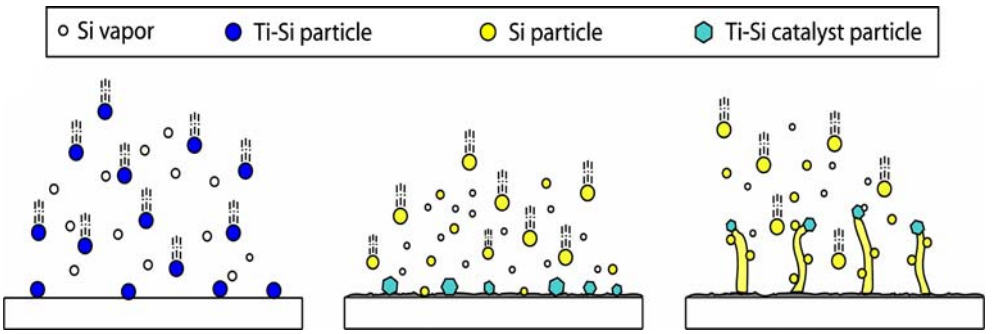

Figure 9. Illustration of proposed growth mechanism. (a) In first step of process, Ti–Si nanoparticles bombard substrate, creating a nanoparticle film. (b) In second step, $TiSi_2$ catalyst particles grow by high-temperature sintering. (c) Nanowires grow by Si vapor deposition and are coated by bombarding Si nanoparticles.

particles are clean, with the possible exception of the crystallite edges, as seen in Figure 4. Once nanoparticles stick to the nanowires, the particles may continue to grow by addition of Si atoms from the vapor.

The above mechanism is admittedly speculative and further experiments will be required to test its validity. Regardless of whether the proposed mechanism is correct, it might be possible to create arbitrary nanoparticle-nanowire material combinations by first growing the nanowires (assuming that this involves a material that is amenable to nanowire growth) and then coating the nanowires with nanoparticles by hypersonic impaction. As this is a high-rate process, and amenable to scale-up, this may suggest a practical route to production of nanoparticle-coated nanowires for various applications.

Conclusions

In summary, a method was developed for the synthesis of Si nanowires densely coated with Si nanoparticles. These structures grow through a combination of chemical vapor deposition and nanoparticle impaction. The catalyst particles are solid crystallites of $TiSi_2$, and the nanowires consist of single-crystal Si. Total process time, including initial deposition of a Ti-rich nanoparticle layer, equaled 5 min, and resulted in formation of a dense network of randomly oriented nanowires covering $\sim$1.5 cm^2 of substrate areas. The diameters of the nanowires vary over the range $\sim$100–800 nm. As a scalable and high-rate deposition process, this method suggests a practical route to production of nanoparticle-coated nanowires for various applications.

Acknowledgements

This work was supported by NSF grant DMI-0103169 and NSF IGERT grant DGE-0114372. We would like to thank Ray Twesten for analytical TEM and corresponding EDS analysis. Twesten's work was carried out at the Center for Microanalysis of Materials, University of Illinois, which is partially supported by the U.S. Department of Energy under grant DEFG02-91-ER45439. In addition we gratefully acknowledge the assistance of Stuart McKernan, of the University of Minnesota Institute of Technology Characterization Facility, in obtaining HRTEM micrographs.

References

Baxter J.B. & E.S. Aydil, 2006. Solar Energy Mater. Solar Cells 90, 601–622.

Bieberich M.T. & S.L. Girshick, 1996. Plasma Chem. Plasma Process. 16, 157S–168S.

Blum J., N. Tymiak, A. Neuman, Z. Wong, N.P. Rao, S.L. Girshick, W.W. Gerberich, P.H. McMurry & J.V.R. Heberlein, 1999. J. Nanoparticle Res. 1, 31–42.

Choi H.C., M. Shim, S. Bangsaruntip & H. Dai, 2002. J. Am. Chem. Soc. 124, 9058–9059.

Gidwani A., 2003. Studies of Flow and Particle Transport in Hypersonic Plasma Particle Deposition and Aerodynamic Focusing. Ph.D. Thesis, University of Minnesota, Minneapolis.

Girshick S.L., J.V.R. Heberlein, P.H. McMurry, W.W. Gerberich, D.I. Iordanoglou, N.P. Rao, A. Gidwani, N. Tymiak, F.D. Fonzo, M.H. Fan & D. Neumann, 2002. Hypersonic plasma particle deposition of nanocrystalline coatings. In: Choy K.L. ed. Innovative Processing of Films and Nanocrystalline Powders. Imperial College Press, London, pp. 165–191.

Jiang K., A. Eitan, L.S. Schadler, P.M. Ajayan, R.W. Siegel, N. Grobert, M. Mayne, M. Reyes-Reyes, H. Terrones & M. Terrones, 2003. Nano Lett. 3, 275–277.

Kamins T.I., R.S. Williams, D.P. Basile, T. Hesjedal & J.S. Harris, 2001. J. Appl. Phys. 89, 1008–1016.

Kamins T.I., R.S. Williams, Y. Chen, Y.L. Chang & Y.A. Chang, 2000. Appl. Phys. Lett. 76, 562–564.

Kolmakov A., D.O. Klenov, Y. Lilach, S. Stemmer & M. Moskovits, 2005. Nano Lett. 5, 667–673.

Kong J., M.G. Chapline & H. Dai, 2001. Adv. Mater. 13, 1384–1386.

LaLonde A.D., M.G. Norton, D.N. McIlroy, D. Zhang, R. Padmanabhan, A. Alkhateeb, H. Han, N. Lane & Z. Holman, 2005. J. Mater. Res. 20, 549–553.

Massalski, T.B., J.L. Murray, L.H. Bennett & H. Baker, (eds.), 1986. Binary Alloy Phase Diagrams. Metals Park, OH: American Society for Metals.

Pan L., K.-K. Lew, J.M. Redwing & E.C. Dickey, 2005. Nano Lett. Web Release Date: 24-May-2005.

Planeix J.M., N. Coustel, B. Coq, V. Brotons, P.S. Kumbhar, R. Dutartre, P. Geneste, P. Bernier & P.M. Ajayan, 1994. J. Am. Chem. Soc. 116, 7935–7936.

Rao C.N.R., F.L. Deepak, G. Gundiah & A. Govindaraj, 2003. Prog. Solid State Chem. 31, 5–147.

Rao N.P., N. Tymiak, J. Blum, A. Neuman, H.J. Lee, S.L. Girshick, P.H. McMurry & J. Heberlein, 1998. J. Aerosol Sci. 29, 707–720.

Tseng R.J., J. Huang, J. Ouyang, R.B. Kaner & Y. Yang, 2005. Nano Lett. 5, 1077–1080.

Wagner R.S. & W.C. Ellis, 1964. Appl. Phys. Lett. 4, 89–90.

Wang N., Y.F. Zhang, Y.H. Tang, C.S. Lee & S.T. Lee, 1998. Appl. Phys. Lett. 73, 3902–3904.

Wang X., J. Hafiz, R. Mukherjee, T. Renault, J. Heberlein, S.L. Girshick & P.H. McMurry, 2005. Plasma Chem. Plasma Process. 25, 439–453.

Ye X.-R., Y. Lin, C. Wang, M.H. Engelhard, Y. Wang & C.M. Wai, 2004. J. Mater. Chem. 14, 908–913.

Ye X.-R., Y. Lin, C. Wang & C.M. Wai, 2003. Adv. Mater. 15, 316–319.

Zhang Y., N.W. Franklin, R.J. Chen & H. Dai, 2000a. Chem. Phys. Lett. 331, 35–41.

Zhang Y., Q. Zhang, Y. Li, N. Wang & J. Zhu, 2000b. Solid State Commun. 115, 51–55.

Zhang Y.F., Y.H. Tang, N. Wang, D.P. Yu, C.S. Lee, T. Bello & S.T. Lee, 1998. Appl. Phys. Lett. 72, 1835–1837.